

DATA OSCILLATION AND CONVERGENCE OF ADAPTIVE FEM*

PEDRO MORIN[†], RICARDO H. NOCHETTO[‡], AND KUNIBERT G. SIEBERT[§]

Abstract. Data oscillation is intrinsic information missed by the averaging process associated with finite element methods (FEM) regardless of quadrature. Ensuring a reduction rate of data oscillation, together with an error reduction based on a posteriori error estimators, we construct a simple and efficient adaptive FEM for elliptic partial differential equations (PDEs) with linear rate of convergence without any preliminary mesh adaptation nor explicit knowledge of constants. Any prescribed error tolerance is thus achieved in a finite number of steps. A number of numerical experiments in two and three dimensions yield quasi-optimal meshes along with a competitive performance.

Key words. a posteriori error estimators, data oscillation, adaptive mesh refinement, convergence, performance, quasi-optimal meshes

AMS subject classifications. 65N12, 65N15, 65N30, 65N50, 65Y20

PII. S0036142999360044

1. Introduction and main result. Adaptive procedures for the numerical solution of partial differential equations (PDEs) started in the late 70's and are now standard tools in science and engineering. We refer to [13] for references on adaptivity of elliptic PDEs, and restrict the list of papers to those strictly related to our work. Adaptive finite element methods (FEM) are indeed a meaningful approach for handling multiscale phenomena and making realistic computations feasible, especially in three dimensions.

A posteriori error estimators are an essential ingredient of adaptivity. They are computable quantities depending on the computed solution(s) and data that provide information about the quality of approximation and may thus be used to make judicious mesh modifications. The ultimate purpose is to construct a sequence of meshes that would eventually equidistribute the approximation errors, and as a consequence the computational effort. To this end, the a posteriori error estimators are split into element indicators which are then employed to make local mesh modifications by refinement and coarsening. This naturally leads to loops of the form

$$(1.1) \quad \text{Solve} \rightarrow \text{Estimate} \rightarrow \text{Refine / Coarsen}.$$

Experience strongly suggests that, starting from a coarse mesh, such an iteration converges within any prescribed error tolerance in a finite number of steps. Except for the rather complete description of the one-dimensional situation by Babuška and

*Received by the editors August 6, 1999; accepted for publication (in revised form) February 2, 2000; published electronically July 19, 2000.

<http://www.siam.org/journals/sinum/38-2/36004.html>

[†]Department of Mathematics, University of Maryland, College Park, MD 20742 (pmorin@math.umd.edu). Permanent Address: Departamento de Matemática, Facultad de Ingeniería Química, Universidad Nacional del Litoral, Argentina. This author was partially supported by Programa FOMEC de la Universidad Nacional del Litoral, CONICET of Argentina, and NSF grants DMS-9623394 and DMS-9971450.

[‡]Department of Mathematics and Institute for Physical Science and Technology, University of Maryland, College Park, MD 20742 (rhn@math.umd.edu). This author was partially supported by NSF grants DMS-9623394 and DMS-9971450.

[§]Institut für Angewandte Mathematik, Hermann-Herder-Str. 10, 79104 Freiburg, Germany (kunibert@mathematik.uni-freiburg.de). This work was developed while this author was visiting the University of Maryland.

Vogelius [2], *convergence* of (1.1) in the multidimensional case is largely an open issue. The fundamental paper [4] of Dörfler for the Poisson equation shows a linear *error reduction* rate for the energy norm towards a preassigned tolerance ϵ in finite steps, provided that

- (a) *the initial mesh is sufficiently refined to resolve data within a tolerance $\mu\epsilon \ll \epsilon$ (mesh fineness);*
- (b) *the sum of the local error indicators of elements marked for refinement amounts to a fixed portion of the global error estimator (marking strategy).*

We also refer to [5] and [6] for related work. Our results are based on, and in fact improve upon, this idea of Dörfler.

To be more specific, let Ω be a polygonal (polyhedral) bounded domain of \mathbb{R}^d , for $d = 2, 3$, and let u be the solution to the following problem:

$$(1.2) \quad \begin{cases} -\operatorname{div}(A \nabla u) = f & \text{in } \Omega, \\ u = 0 & \text{on } \partial\Omega, \end{cases}$$

where $f \in L^2(\Omega)$ and A is a piecewise constant positive definite symmetric matrix. Let \mathcal{T}_H be a conforming triangulation of Ω , with piecewise constant meshsize H , and let u_H denote the piecewise linear finite element solution over \mathcal{T}_H assuming exact integration. This is an ideal situation which helps isolate essential difficulties from quadrature issues; the latter deserve a separate investigation. The following quantity, hereafter called *data oscillation*, will play a fundamental role:

$$(1.3) \quad \operatorname{osc}(f, \mathcal{T}_H) := \left(\sum_{T \in \mathcal{T}_H} \|H(f - f_T)\|_T^2 \right)^{1/2};$$

from now on f_T stands for the mean value of f over T , but may be any piecewise constant approximation to f on T . Such $\operatorname{osc}(f, \mathcal{T}_H)$ measures intrinsic information missing in the averaging process associated with finite elements, which fail to detect fine structures of f . We stress that (1.3) is unrelated to quadrature and quantifies data oscillation with the least amount of information per element, namely one degree of freedom associated with f_T .

In contrast to [4], which imposes the constraint $(\sum_{T \in \mathcal{T}_H} \|Hf\|_T^2)^{1/2} \leq \mu\epsilon$ on the interior residual as a notion of mesh fineness in (a), we claim that $\operatorname{osc}(f, \mathcal{T}_H) \leq \mu\epsilon$ is what really matters; this crucial property is derived in section 4. We observe that $\operatorname{osc}(f, \mathcal{T}_H)$ is generically of higher order than the interior residual, and so (a) is easier to obtain whereas the original condition of [4] may easily lead to an initial overrefinement (see section 5.2). As illustrated in Example 3.7, there might be pathological instances when data oscillation and interior residual are comparable and the concept of mesh fineness becomes relevant. To circumvent the restriction of mesh fineness, we propose simple but essential changes to [4] which result in a practical procedure, Algorithm C of section 3, whose formulation needs no tolerance ϵ . In addition to marking elements according to (b) in each step, Algorithm C starts from any coarse mesh and ensures one interior node for each marked element together with a linear data oscillation decay. The interior node guarantees suitable error decrease when data oscillation is relatively small. Its need is justified in Examples 3.5 and 3.6, and a proof of the fundamental error reduction property is given in section 4. Algorithm C yields the following convergence result, proved in section 3.

Main result. *Let u_k be a sequence of finite element solutions produced by Algorithm C. There exist positive constants C_0 and $\beta < 1$, depending only on given data and the initial grid, such that*

$$(1.4) \quad \|u - u_k\|_{\Omega} \leq C_0 \beta^k,$$

where the energy norm is given by $\|v\|_{\Omega} = (\int_{\Omega} \nabla v \cdot A \nabla v)^{1/2}$. The initial coarse mesh need not be adjusted to resolve data to any tolerance, and no explicit constants are needed for Algorithm C to work.

A few comments and comparisons are now in order.

- Any prescribed error tolerance ϵ may be met in finite steps, as in [4], but without any special tuning of the initial mesh in terms of ϵ ; this issue is important and its practical implications are fully examined in section 5.2.
- Depending on the flatness of u , the meshsize H may not necessarily tend to zero, which makes this a nonstandard finite element asymptotic statement.
- Even though no stability constants are required for Algorithm C, nor for convergence, the constant in the upper bound of the residual-type a posteriori error estimate is needed to stop the iterations; this is customary in adaptivity [13].
- Inequality (1.4) does not imply that the error decays in every single step as in [4], and Example 3.7 shows that it may be constant for a number of steps due to unresolved data oscillation.
- The interior node created by Algorithm C guarantees suitable error decrease when data oscillation is small and is discussed in Examples 3.5 and 3.6. This theoretical requirement may be viewed as a looking-ahead strategy, and the two- and three-dimensional experiments of section 5 clearly indicate no additional computational expense.

In section 5 we present several illuminating numerical experiments computed within the finite element toolbox ALBERT [11, 12]. The first example is the crack problem, which exhibits a point singularity of the form $r^{1/2}$. The second example corresponds to intersecting interfaces (discontinuous coefficients) and a much more severe singularity of the form r^{γ} with γ arbitrarily close to 0. In both cases f is constant and thus $\text{osc}(f, \mathcal{T}_H) = 0$. We finally discuss a two- and three-dimensional example with variable f and thereby test the effect of data oscillation. It turns out that this effect seems to play a minor role for smooth f (relative to the underlying mesh). This provides a heuristic explanation for the success of most adaptive strategies which disregard the issue of data oscillation altogether. The experiments also reveal that the resulting meshes are quasi-optimal: the error decays proportionally to $N^{-1/d}$, N being the number of degrees of freedom. Our theory, however, does not explain this important property. Mesh optimality has been recently studied in [3] via wavelet algorithms which resort to the entire wavelet expansions of u and f . These full expansions are not available in practice though and somehow encode the missing information of data oscillation.

This paper is organized as follows. In section 2 we recall the standard a posteriori residual-type error estimators which constitute the core of adaptivity [13]. In section 3 we present Algorithm C, justify its various steps, and prove the main result. In section 4 we derive the crucial error reduction property, thereby closing the gap. We conclude with several two- and three-dimensional experiments in section 5 which fully document the competitive performance of our novel adaptive strategy.

2. A posteriori error estimators. We start this section with some useful notation. For an open set $G \subset \mathbb{R}^d$ we denote by $H^1(G)$ the usual Sobolev space of functions in $L^2(G)$ whose first derivatives are also in $L^2(G)$, endowed with the norm

$$\|u\|_{H^1(G)} := (\|u\|_G^2 + \|\nabla u\|_G^2)^{1/2},$$

where $\|\cdot\|_G$ stands for the $L^2(G)$ -norm.

Since A is piecewise constant, symmetric, and positive definite, the bilinear form $((\cdot, \cdot))_G$ defined for any open set $G \subset \Omega$ by

$$((u, v))_G := \int_G A \nabla u \cdot \nabla v$$

is bounded, and $((\cdot, \cdot))_\Omega$ is coercive on $H_0^1(\Omega)$, i.e., there exist constants $0 < c_a \leq C_a < \infty$ such that

$$(2.1) \quad ((v, w))_G \leq C_a \|v\|_{H^1(G)} \|w\|_{H^1(G)} \quad \forall v, w \in H^1(G),$$

$$(2.2) \quad c_a \|v\|_{H^1(\Omega)}^2 \leq ((v, v))_\Omega \quad \forall v \in H_0^1(\Omega).$$

This implies, in particular, that the seminorm $\|\cdot\|_G$ defined by $\|v\|_G^2 := ((v, v))_G$ is equivalent to the $H_0^1(\Omega)$ -norm when $G = \Omega$.

In view of (2.1) and (2.2), problem (1.2) admits a unique weak solution u for any $f \in L^2(\Omega)$, i.e.,

$$(2.3) \quad u \in H_0^1(\Omega) : \quad ((u, v))_\Omega = \int_\Omega f v \quad \forall v \in H_0^1(\Omega).$$

Let \mathcal{T}_H be a conforming regular triangulation of Ω , with piecewise constant mesh-size H , i.e., $H|_T = \text{diam}(T)$. Let \mathbb{V}^H be the space of continuous piecewise linear functions over \mathcal{T}_H , and let \mathbb{V}_0^H be the subspace of functions of \mathbb{V}^H that vanish at the boundary. Let u_H denote the solution of the discrete problem

$$(2.4) \quad u_H \in \mathbb{V}_0^H : \quad ((u_H, \phi))_\Omega = \int_\Omega f \phi \quad \forall \phi \in \mathbb{V}_0^H.$$

The function f_H will denote the piecewise constant function over \mathcal{T}_H that, restricted to each element $T \in \mathcal{T}_H$, is equal to the mean value f_T of f on T .

We denote by \mathcal{S}_H the set of sides of the triangulation \mathcal{T}_H that do not belong to the boundary $\partial\Omega$ of the domain Ω . For $S \in \mathcal{S}_H$, the domain Ω_S is the union of the two elements in \mathcal{T}_H sharing S , and H_S denotes the diameter of S . We assume that all partitions \mathcal{T}_H match the discontinuities of A , i.e., the jumps of A are located on interelement boundaries $S \in \mathcal{S}_H$.

We now recall the *residual-type* a posteriori error estimators for (2.3) and (2.4) [1], [13]. Subtracting (2.4) from (2.3) and integrating by parts yields the following well-known relation between the error $u - u_H$ and the residuals:

$$(2.5) \quad ((u - u_H, \phi)) = \sum_{T \in \mathcal{T}_H} \int_T f(\phi - \mathcal{I}_H \phi) + \sum_{S \in \mathcal{S}_H} \int_S J_S(\phi - \mathcal{I}_H \phi)$$

for all $\phi \in H_0^1(\Omega)$. Hereafter, \mathcal{I}_H denotes the Clément interpolation operator, and $J_S = [A \nabla u_H]_S \cdot \nu$ represents the jump of flux across side S which is independent of

the orientation of the unit normal ν . Let η_S be the (local) error indicator associated with side $S \in \mathcal{S}_H$

$$(2.6) \quad \eta_S^2 := \left\| H_S^{\frac{1}{2}} J_S \right\|_S^2 + \|H f\|_{\Omega_S}^2,$$

which consists of the jump and interior residuals, respectively. Let η_H be the (global) error estimator given by

$$\eta_H^2 := \sum_{S \in \mathcal{S}_H} \eta_S^2.$$

Upon taking $\phi = u - u_H$ in (2.5), and using interpolation theory, the following result emerges [1], [13].

LEMMA 2.1 (upper bound). *There exists a constant C_1 , depending only on the minimum angle of \mathcal{T}_H , C_a , and c_a , such that*

$$(2.7) \quad \|u - u_H\|_{\Omega}^2 \leq C_1 \eta_H^2.$$

An early indication of the crucial role of oscillation is given by the (local) lower bound [1], [13]. The construction by Verfürth [13] will be important later.

LEMMA 2.2 (lower bound). *There exist constants C_2, C_3 , depending only on the minimum angle of \mathcal{T}_H , C_a , and c_a , such that*

$$(2.8) \quad C_2 \eta_S^2 - C_3 \|H(f - f_H)\|_{\Omega_S}^2 \leq \|u - u_H\|_{\Omega_S}^2.$$

Remark 2.3. Suppose that $\|H(f - f_H)\|_{\Omega_S}$ is small with respect to η_S . In such a case, the significance of (2.8) is that the size of η_S provides reliable information about the size of $\|u - u_H\|_{\Omega_S}$. This explains why refining elements with large error indicators usually tends to equidistribute approximation errors, an ultimate goal of adaptivity.

Remark 2.4. It is worth realizing that f_H in (2.8) could be any piecewise polynomial and not just the mean value of f over the elements. This additional freedom in measuring data oscillation disappears in dealing with consecutive discrete solutions u_H and u_h . This issue will be central to our discussions of section 4.

3. Algorithm C and convergence. We start with a marking strategy for *error reduction* due to Dörfler [4]:

Marking Strategy E

Given a parameter $0 < \theta < 1$:

1. Construct a subset $\hat{\mathcal{S}}_H$ of \mathcal{S}_H such that

$$\left(\sum_{S \in \hat{\mathcal{S}}_H} \eta_S^2 \right)^{1/2} \geq \theta \eta_H.$$
2. Let $\hat{\mathcal{T}}_H$ be the set of elements with one side in $\hat{\mathcal{S}}_H$ and mark all these elements.

This marking strategy ensures that we choose sufficiently many sides S such that their contributions η_S constitute a fixed proportion of the global error estimator η_H . Using Marking Strategy E, we have the following error reduction result which is proved in section 4.

THEOREM 3.1 (error reduction). *Let \mathcal{T}_H be a triangulation of Ω , and let $\hat{\mathcal{T}}_H$ and $\hat{\mathcal{S}}_H$ be as defined in Marking Strategy E. Let \mathcal{T}_h be a refinement of \mathcal{T}_H satisfying:*

$$(3.1) \quad \text{each element of } \hat{\mathcal{T}}_H, \text{ as well as each side in } \hat{\mathcal{S}}_H, \text{ contains a node of } \mathcal{T}_h \text{ in its interior.}$$

Then there exist constants $\mu > 0$ and $0 < \alpha < 1$, depending only on the minimum angle, θ , C_a , and c_a , such that for any $\epsilon > 0$, if

$$(3.2) \quad \text{osc}(f, \mathcal{T}_H) \leq \mu\epsilon,$$

then either $\|u - u_H\|_\Omega \leq \epsilon$ or the solution u_h on the mesh \mathcal{T}_h satisfies

$$\|u - u_h\|_\Omega \leq \alpha \|u - u_H\|_\Omega.$$

Remark 3.2. This result establishes an error reduction provided the current error is larger than the desired tolerance ϵ . In [4], Dörfler proves a similar result assuming that $(\sum_{T \in \mathcal{T}_H} \|Hf\|_T^2)^{1/2} \leq \mu\epsilon$ instead of (3.2). The notion of *mesh fineness* given by (3.2) is generically of higher order than the one given in [4].

Remark 3.3. The requirement of having a node of the refined grid \mathcal{T}_h inside each marked element of \mathcal{T}_H is an essential difference with [4]. This requirement is responsible for the new measure of data approximation. Its implementation in two and three dimensions by bisection is discussed in section 5.

Remark 3.4. A repeated application of Marking Strategy E, and the special refinement (3.1) of Theorem 3.1, lead to an iterative process that converges in a finite number of steps to a discrete solution within tolerance ϵ ; this is the main contribution of [4]. However, if this process were to be restarted with a stringent tolerance, data oscillation might not satisfy (3.2). Consequently, this strategy alone does *not* yield an asymptotically convergent algorithm.

To shed light on the ingredients for convergence, we discuss three examples. They show the importance of the special refinement of Theorem 3.1 with an interior node to obtain an error reduction, as well as the necessity of controlling data oscillation.

Example 3.5 (interior node 1). This example shows the necessity of creating an interior node inside each refined triangle. Consider problem (1.2) with $A = Id$, $f \equiv 1$, and $\Omega = (0, 1) \times (0, 1)$. Let $\{(0, 0), (1, 0), (1, 1), (0, 1), (\frac{1}{2}, \frac{1}{2})\}$ be the set of vertices of \mathcal{T}_H (see Figure 3.1).

Now let us call ϕ_1 the nodal basis function of \mathbb{V}^H that corresponds to the node $(\frac{1}{2}, \frac{1}{2})$. Then the finite element solution u_H on this grid is $c_1\phi_1$, where

$$c_1 \int_{\Omega} \nabla \phi_1 \cdot \nabla \phi_1 = \int_{\Omega} f \phi_1 \quad \Rightarrow \quad c_1 = \frac{1/3}{4} = \frac{1}{12}.$$

Let \mathcal{T}_h be the grid obtained from \mathcal{T}_H by performing two bisections on each triangle of \mathcal{T}_H using the newest-vertex bisection and assuming that $(\frac{1}{2}, \frac{1}{2})$ is the newest vertex on the initial grid. This is the standard refinement performed in [4] and does not lead to an interior node in the refined elements (see Figure 3.1). Then we get a larger set of nodes, which we enumerate as in Figure 3.1. Let us call φ_i the nodal basis function of \mathbb{V}^h that corresponds to the node i of \mathcal{T}_h , $i = 1, 2, \dots, 5$. The finite element solution u_h on this refined grid is $u_h = \sum_{i=1}^5 c_i \varphi_i$, where $c := (c_i)_{i=1}^5$ satisfies the equation

$Kc = b$, with K and b given by

$$K = \begin{bmatrix} 4 & 0 & -1 & 0 & 0 \\ 0 & 4 & -1 & 0 & 0 \\ -1 & -1 & 4 & -1 & -1 \\ 0 & 0 & -1 & 4 & 0 \\ 0 & 0 & -1 & 0 & 4 \end{bmatrix} \quad \text{and} \quad b = \begin{bmatrix} 1/12 \\ 1/12 \\ 1/6 \\ 1/12 \\ 1/12 \end{bmatrix},$$

which gives $c = (\frac{1}{24}, \frac{1}{24}, \frac{1}{12}, \frac{1}{24}, \frac{1}{24})^t$, and consequently, $u_h = u_H$. This equality implies that the errors corresponding to both grids \mathcal{T}_H and \mathcal{T}_h are equal. We conclude that without one interior node in at least one triangle, no error reduction is obtained even when $\text{osc}(f, \mathcal{T}_H) = 0$ and $\|u - u_H\|_\Omega > 0$.

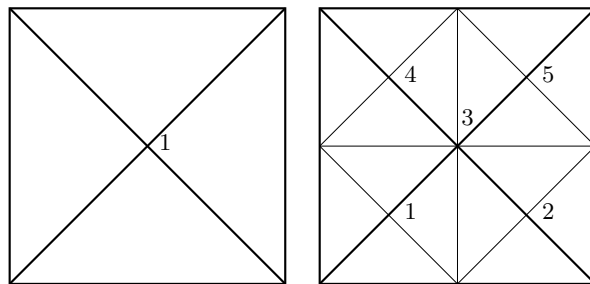


FIG. 3.1. Refinement by bisecting all triangles twice.

Example 3.6 (interior node 2). At first sight, it may seem that the situation of Example 3.5 may occur only at the first refinement step. This example shows that such a situation can also happen at any refinement step n .

Fix $n \in \mathbb{N}$ and consider (1.2) with $A = Id$, $\Omega = (0, 1)^2$, and f given by

$$f(x) = \begin{cases} 1 & \text{if } x \in (i2^{-n}, (i+1)2^{-n}) \times (j2^{-n}, (j+1)2^{-n}) \text{ and } i+j \text{ odd} \\ -1 & \text{otherwise;} \end{cases}$$

see Figure 3.2. Then, if we start with \mathcal{T}_0 equal to the grid \mathcal{T}_H of Example 3.5, and ϕ_1 also as in Example 3.5, we have that ϕ_1 is orthogonal to f and consequently $u_0 \equiv 0$. If we now define recursively \mathcal{T}_{k+1} , $k = 0, 1, \dots$ as the grid that results from \mathcal{T}_k by performing two newest-vertex bisections on every triangle (see Figure 3.2), we will have $u_k \equiv 0$ for $k = 0, 1, \dots, n - 1$, due to the fact that f is orthogonal to the basis functions of \mathcal{T}_k for $k = 0, 1, \dots, n - 1$.

For $k = n$ the solution u_n will not be zero anymore, but it will be zero along the lines where f changes sign due to the symmetry of the problem, and the same will happen with u_{n+1} . Then, if we observe u_n and u_{n+1} in a fixed square where f is constant, they behave exactly as u_H and u_h do in Example 3.5, and consequently $u_n = u_{n+1}$, which means that the error does not decrease, even when the oscillation $\text{osc}(f, \mathcal{T}_n)$ is zero.

Example 3.7 (data oscillation). This example shows that if the data oscillation $\text{osc}(f, \mathcal{T}_H)$ is not small, then, even introducing an interior node on all elements, the error may not decrease. To see this, consider Example 3.6 for some fixed large $n \in \mathbb{N}$. Observe now that if we obtain \mathcal{T}_{k+1} by performing *three* bisections on all the elements

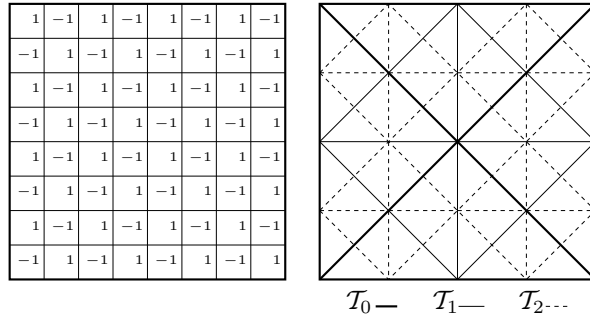


FIG. 3.2. Values of the function f of Example 3.6 for $n = 3$ (left), and grids \mathcal{T}_k for $k = 0, 1, 2$ (right).

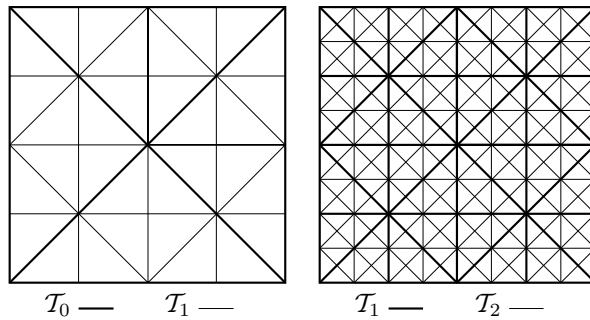


FIG. 3.3. Resulting grid \mathcal{T}_1 (left) and \mathcal{T}_2 (right) after performing three bisections on each element of \mathcal{T}_0 and \mathcal{T}_1 , respectively.

of \mathcal{T}_k , then three new nodes are created on the edge opposite to the newest vertex in addition to an interior node per element (see Figure 3.3). Even though this refinement is stronger than required by Theorem 3.1 in each step, the solutions, u_k will all be zero for $k < 2n/3$.

We conclude from Examples 3.5 and 3.6 that the interior node is necessary to obtain an error decrease, and from Example 3.7 that this may not be sufficient if the mesh does not resolve the oscillation of data. Therefore, in order to obtain an asymptotically convergent sequence of discrete solutions, we must readjust the mesh to resolve $\text{osc}(f, \mathcal{T}_H)$ according to a decreasing tolerance. The following simple results guarantee that this is always possible. The first lemma considers the worst scenario situation of f just in $L^2(\Omega)$, whereas the second lemma addresses the case of f piecewise smooth.

LEMMA 3.8. Let $0 < \gamma < 1$ be the reduction factor of element size associated with one refinement step. Given $0 < \hat{\theta} < 1$, let $\hat{\alpha} := (1 - (1 - \gamma^2)\hat{\theta}^2)^{1/2}$. Let $\hat{\mathcal{T}}_H$ be a subset of \mathcal{T}_H such that

$$(3.3) \quad \text{osc}(f, \hat{\mathcal{T}}_H) \geq \hat{\theta} \text{osc}(f, \mathcal{T}_H).$$

If \mathcal{T}_h is a triangulation obtained from \mathcal{T}_H by refining at least every element in $\hat{\mathcal{T}}_H$, then the following data oscillation reduction occurs:

$$(3.4) \quad \text{osc}(f, \mathcal{T}_h) \leq \hat{\alpha} \text{osc}(f, \mathcal{T}_H).$$

Proof. Let $T \in \mathcal{T}_h$ be an element contained in $\hat{T} \in \hat{\mathcal{T}}_H$. Since $f_T = |T|^{-1} \int_T f$ is the L^2 -projection of f onto the space of piecewise constants over T , we have

$$\|f - f_T\|_T \leq \|f - f_{\hat{T}}\|_T.$$

Since $h_T \leq \gamma h_{\hat{T}}$, we discover that

$$\begin{aligned} \text{osc}(f, \mathcal{T}_h)^2 &= \sum_{T \in \mathcal{T}_h} h_T^2 \|f - f_T\|_T^2 \\ &\leq \gamma^2 \sum_{\hat{T} \in \hat{\mathcal{T}}_H} h_{\hat{T}}^2 \|f - f_{\hat{T}}\|_{\hat{T}}^2 + \sum_{T \in \mathcal{T}_H \setminus \hat{\mathcal{T}}_H} h_T^2 \|f - f_T\|_T^2 \\ &= (\gamma^2 - 1) \text{osc}(f, \hat{\mathcal{T}}_H)^2 + \text{osc}(f, \mathcal{T}_H)^2 \leq \hat{\alpha}^2 \text{osc}(f, \mathcal{T}_H)^2. \quad \square \end{aligned}$$

LEMMA 3.9. *Let f be piecewise H^s for $0 < s \leq 1$ over the initial mesh, where H^s stands for the space of functions f with fractional derivative $D^s f$ of order s in L^2 . Let data oscillation be redefined by*

$$\text{osc}(f, \mathcal{T}_h) := \left(\sum_{T \in \mathcal{T}_h} h_T^{2+2s} \|D^s f\|_T^2 \right)^{1/2}.$$

Let $\hat{\alpha} := (1 - (1 - \gamma^{2+2s})\hat{\theta}^2)^{1/2}$, where γ and $\hat{\theta}$ are defined in Lemma 3.8. If \mathcal{T}_h is as in Lemma 3.8, then

$$(3.5) \quad \text{osc}(f, \mathcal{T}_h) \leq \hat{\alpha} \text{osc}(f, \mathcal{T}_H).$$

Proof. It suffices to use that $h_T \leq \gamma h_{\hat{T}}$ for all $T \in \mathcal{T}_h$ contained in $\hat{T} \in \hat{\mathcal{T}}_H$ and argue as in Lemma 3.8. \square

We point out that γ depends only on the minimal angle of the initial mesh, and that $\gamma \leq 1/2$ in two dimensions provided one interior node is created per marked element; we refer to Figure 5.1 of section 5. This implies that the reduction rate squared of Lemma 3.9 is $\hat{\alpha}^2 \leq 1 - 15\hat{\theta}^2/16 \approx 1 - \hat{\theta}^2$ in two dimensions provided f is piecewise H^1 .

Taking into account that a subset $\hat{\mathcal{T}}_H$ of \mathcal{T}_H is already selected by Marking Strategy E, the following procedure, in conjunction with Lemmas 3.8 or 3.9, guarantees a *data oscillation* decrease by a factor $\hat{\alpha} < 1$.

Marking Strategy D

Given a parameter $0 < \hat{\theta} < 1$ and the subset $\hat{\mathcal{T}}_H \subset \mathcal{T}_H$ produced by Marking Strategy E:

1. Enlarge $\hat{\mathcal{T}}_H$ such that

$$\text{osc}(f, \hat{\mathcal{T}}_H) \geq \hat{\theta} \text{osc}(f, \mathcal{T}_H).$$
2. Mark all elements in $\hat{\mathcal{T}}_H$ for refinement.

In light of Theorem 3.1, Examples 3.5, 3.6, and 3.7, and Lemmas 3.8 and 3.9, we are now in the position to formulate Algorithm C and prove its asymptotic convergence.

Convergent Algorithm C

Choose parameters $0 < \theta, \hat{\theta} < 1$.

1. Pick up any initial mesh \mathcal{T}_0 such that A is piecewise constant over \mathcal{T}_0 .
2. Solve the system on \mathcal{T}_0 for the discrete solution u_0 .
3. Let $k = 0$.
4. Compute the local indicators η_S .
5. Construct $\hat{\mathcal{T}}_k \subset \mathcal{T}_k$ by Marking Strategy E and parameter θ .
6. Enlarge $\hat{\mathcal{T}}_k$ by Marking Strategy D and parameter $\hat{\theta}$.
7. Let \mathcal{T}_{k+1} be a refinement of \mathcal{T}_k such that each element of $\hat{\mathcal{T}}_k$, as well as each of its sides, contains a node of \mathcal{T}_{k+1} in its interior.
8. Solve the system on \mathcal{T}_{k+1} for the discrete solution u_{k+1} .
9. Let $k = k + 1$ and go to Step 4.

Remark 3.10. To create an interior node for each element of $\hat{\mathcal{T}}_k$ we use a bisection algorithm, which also produces, as a by-product, at least one interior node in each of the element sides (see section 5.1).

THEOREM 3.11 (convergence). *For $0 < \theta, \hat{\theta} < 1$, let $0 < \alpha < 1$, $\mu > 0$ be given by Theorem 3.1 and $0 < \hat{\alpha} < 1$ by Lemmas 3.8 or 3.9. Let*

$$(3.6) \quad \beta := \max(\alpha, \hat{\alpha}), \quad C_0 := \max\left(\|u - u_0\|_{\Omega}, \frac{\text{osc}(f, \mathcal{T}_0)}{\alpha\mu}\right).$$

Algorithm C produces a convergent sequence $\{u_k\}_{k \in \mathbb{N}_0}$ of discrete solutions satisfying for all $k \geq 0$

$$(3.7) \quad \|u - u_k\|_{\Omega} \leq C_0 \beta^k.$$

Proof. We argue by induction. Such a bound holds trivially for $k = 0$. We assume that (3.7) holds for k . Then we have either

$$(i) \quad \|u - u_k\|_{\Omega} > C_0 \beta^{k+1} \quad \text{or} \quad (ii) \quad \|u - u_k\|_{\Omega} \leq C_0 \beta^{k+1}.$$

In case (i), we see from step 6 of Algorithm C that $\text{osc}(f, \mathcal{T}_k) \leq \hat{\alpha}^k \text{osc}(f, \mathcal{T}_0) \leq \beta^k \text{osc}(f, \mathcal{T}_0)$ and, consequently, that for $\epsilon := C_0 \beta^{k+1}$

$$\text{osc}(f, \mathcal{T}_k) \leq \mu C_0 \alpha \beta^k \leq \mu C_0 \beta^{k+1} = \mu \epsilon.$$

Since $\|u - u_k\|_{\Omega} > \epsilon$, we may then combine Theorem 3.1 with (3.7) to arrive at

$$\|u - u_{k+1}\|_{\Omega} \leq \beta \|u - u_k\|_{\Omega} \leq C_0 \beta^{k+1}.$$

On the other hand, exploiting that \mathcal{T}_{k+1} is a refinement of \mathcal{T}_k , and thus the error must not increase, we can handle case (ii) as follows:

$$\|u - u_{k+1}\|_{\Omega} \leq \|u - u_k\|_{\Omega} \leq C_0 \beta^{k+1}.$$

This completes the induction procedure and the proof. \square

Remark 3.12. Algorithm C is fully practical in that it needs only parameters $\theta, \hat{\theta}$. The unknown constants $\alpha, \hat{\alpha}$ and μ are not explicitly needed by Algorithm C, but they dictate the convergence rate.

Remark 3.13. Stopping the sequence $\{u_k\}$ to achieve an error tolerance is the only instance that requires the constant C_1 of Lemma 2.1. This difficulty, associated with residual-type estimators, is customary in the literature though.

Remark 3.14. In view of Lemma 3.9 we expect data oscillation to yield rather minor additional refinement to step 5. This is confirmed by the numerical experiments of section 5.4 in both two and three dimensions, and provides some solid theoretical grounds for the convergence of adaptive strategies which disregard data oscillation altogether.

4. Error reduction. In this section we prove Theorem 3.1. The following orthogonality result is essential and gives us an idea of how to proceed.

LEMMA 4.1. *If \mathcal{T}_h is a local refinement of \mathcal{T}_H , such that $\mathbb{V}^H \subset \mathbb{V}^h$, the following relation holds:*

$$(4.1) \quad \|u - u_h\|_\Omega^2 = \|u - u_H\|_\Omega^2 - \|u_H - u_h\|_\Omega^2.$$

Proof. By Galerkin orthogonality, $((u - u_h, v))_\Omega = 0$ for all $v \in \mathbb{V}^h$, whence $u_h - u_H \in \mathbb{V}^h$ is perpendicular to $u - u_h$. Therefore, since $u - u_H = (u - u_h) + (u_h - u_H)$, the assertion (4.1) follows from the Pythagoras' theorem. \square

We can see from this lemma that the error reduction is exactly $\|u_H - u_h\|_\Omega^2$. In order to guarantee that the error decreases a fixed proportion of the current error, we have to bound $\|u_H - u_h\|_\Omega^2$ from below by $\|u - u_H\|_\Omega^2$. In view of Lemma 2.2, this reduces to show a lower bound in terms of η_H^2 . The following lemma establishes a *local* lower bound for the error decrease in terms of the *local error indicators*. This result will be needed, in conjunction with Lemma 2.1, to prove a *global lower bound* of the error decrease in terms of the current error.

LEMMA 4.2. *Let \mathcal{T}_H be a triangulation of Ω , and let $\hat{\mathcal{T}}_H$ and $\hat{\mathcal{S}}_H$ be as defined in Marketing Strategy E. Let \mathcal{T}_h be a refinement of \mathcal{T}_H satisfying (3.1). Then there exist constants C_4, C_5 , depending only on the minimum angle and c_a, C_a , such that*

$$(4.2) \quad \eta_S^2 \leq C_4 \|u_h - u_H\|_{\Omega_S}^2 + C_5 \|H(f - f_H)\|_{\Omega_S}^2 \quad \forall S \in \hat{\mathcal{S}}_H.$$

Before getting into the proof of this lemma, observe that this result is similar to the result of Lemma 2.2. Their main differences are that here we get a lower bound for $\|u_h - u_H\|_{\Omega_S}$ instead of $\|u - u_H\|_{\Omega_S}$, and that f_H stands for a piecewise *constant* approximation of f , i.e., f_H has only one degree of freedom in each triangle $T \in \mathcal{T}_H$.

Proof of Lemma 4.2. We split the proof into several steps.

(1) We claim that there exists an auxiliary function $\phi \in \mathbb{V}^h$, satisfying $\phi|_{\partial\Omega_S} = 0$ together with the two conditions

$$(4.3) \quad \int_{\Omega_S} f_H \phi + \int_S J_S \phi = \|H f_H\|_{\Omega_S}^2 + \|H_S^{\frac{1}{2}} J_S\|_S^2,$$

$$(4.4) \quad \|\nabla \phi\|_{\Omega_S}^2 \leq C \left(\|H f_H\|_{\Omega_S}^2 + \|H_S^{\frac{1}{2}} J_S\|_S^2 \right),$$

where the constant C depends only on the minimum angle. We postpone the construction of ϕ and show first how to exploit it.

(2) Since $\phi \in \mathbb{V}^h$ and vanishes on $\partial\Omega_S$, integration by parts yields

$$\begin{aligned} ((u_h - u_H, \phi))_{\Omega_S} &= \int_{\Omega_S} f \phi + \int_S J_S \phi \\ &= \int_{\Omega_S} f_H \phi + \int_S J_S \phi + \int_{\Omega_S} (f - f_H) \phi. \end{aligned}$$

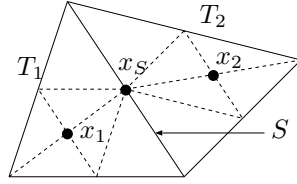


FIG. 4.1. Example of a refined two-element patch $\Omega_S = T_1 \cup T_2$ in two dimensions.

Using (2.1) and (4.3), the Poincaré inequality $\|\phi\|_{\Omega_S} \leq CH_S \|\nabla\phi\|_{\Omega_S}$, we obtain

$$\begin{aligned} \|Hf_H\|_{\Omega_S}^2 + \|H_S^{\frac{1}{2}}J_S\|_S^2 &= ((u_h - u_H, \phi))_{\Omega_S} - \int_{\Omega_S} (f - f_H)\phi \\ &\leq \|u_h - u_H\|_{\Omega_S} \|\phi\|_{\Omega_S} + \|f - f_H\|_{\Omega_S} \|\phi\|_{\Omega_S} \\ &\leq C (\|u_h - u_H\|_{\Omega_S} + \|H(f - f_H)\|_{\Omega_S}) \|\nabla\phi\|_{\Omega_S}. \end{aligned}$$

In view of (4.4) we thus obtain

$$\|Hf_H\|_{\Omega_S}^2 + \|H_S^{\frac{1}{2}}J_S\|_S^2 \leq C \|u_h - u_H\|_{\Omega_S}^2 + C \|H(f - f_H)\|_{\Omega_S}^2.$$

(3) By virtue of this and the triangle inequality, we get

$$\begin{aligned} \eta_S^2 &= \|H_S^{\frac{1}{2}}J_S\|_S^2 + \|Hf\|_{\Omega_S}^2 \\ &\leq 2 \left(\|H_S^{\frac{1}{2}}J_S\|_S^2 + \|Hf_H\|_{\Omega_S}^2 + \|H(f - f_H)\|_{\Omega_S}^2 \right) \\ &\leq C_4 \|u_h - u_H\|_{\Omega_S}^2 + C_5 \|H(f - f_H)\|_{\Omega_S}^2, \end{aligned}$$

which proves the assertion (4.2).

(4) To complete the proof it remains to construct ϕ . To do so, let $\varphi_S, \varphi_1,$ and φ_2 be the nodal basis functions of \mathbb{V}^h which are equal to one at the interior nodes x_S of S , and x_1, x_2 of T_1 and T_2 , respectively; here T_1 and T_2 denote the two elements of \mathcal{T}_H sharing S (see Figure 4.1). The existence of x_1, x_2 and x_S is guaranteed by step 7 of Algorithm C. Next, consider $\phi = \alpha_S\varphi_S + \beta_1\varphi_1 + \beta_2\varphi_2$, where the constants $\alpha_S, \beta_1,$ and β_2 will be determined later. If $f_i := f_{T_i}$ and $H_i := H_{T_i}$, we can write

$$(4.5) \quad \int_{\Omega_S} f_H\phi + \int_S J_S\phi = \alpha_S \int_S J_S\varphi_S + \sum_{i=1,2} \left(\beta_i \int_{T_i} f_i\varphi_i + \alpha_S \int_{T_i} f_i\varphi_S \right),$$

because the supports of φ_1 and φ_2 do not overlap. Since choosing

$$\alpha_S = \begin{cases} \frac{\|H_S^{\frac{1}{2}}J_S\|_S^2}{\int_S J_S\varphi_S} & \text{if } J_S \neq 0, \\ 0 & \text{otherwise,} \end{cases} \quad \text{and } \beta_i = \begin{cases} \frac{\|H_i f_i\|_{T_i}^2 - \alpha_S \int_{T_i} f_i\varphi_S}{\int_{T_i} f_i\varphi_i} & \text{if } f_i \neq 0, \\ 0 & \text{otherwise,} \end{cases}$$

for $i = 1, 2$, the condition (4.3) is satisfied, it only remains to prove (4.4). To this end, we observe first that

$$\|\nabla\phi\|_{\Omega_S} \leq |\alpha_S| \|\nabla\varphi_S\|_{\Omega_S} + \sum_{i=1,2} |\beta_i| \|\nabla\varphi_i\|_{\Omega_S},$$

and estimate each term on the right-hand side separately. If $J_S \neq 0$, using that H_S and J_S are constant, as well as $\|\nabla\varphi_S\|_{\Omega_S} \leq CH_S^{-1}$, we get

$$|\alpha_S| \|\nabla\varphi_S\|_{\Omega_S} = dH_S|J_S| \|\nabla\varphi_S\|_{\Omega_S} \leq Cd \left\| H_S^{\frac{1}{2}} J_S \right\|_S,$$

where C is a constant depending only on the minimum angle of \mathcal{T}_h and d is the dimension. A similar bound is valid with φ_S replaced by φ_i . Likewise, using now that f_i is constant, we have for $f_i \neq 0$

$$|\beta_i| \leq \frac{\int_{T_i} H_i^2 f_i^2}{\int_{T_i} |f_i| \varphi_i} + \frac{|\alpha_S| \int_{T_i} |f_i| \varphi_S}{\int_{T_i} |f_i| \varphi_i} \leq CH_i^2 |f_i| + C|\alpha_S|,$$

with C depending on d and the minimum angle of \mathcal{T}_h . Then

$$|\beta_i| \|\nabla\varphi_i\|_{\Omega_S} \leq CH_i^2 |f_i| \|\nabla\varphi_i\|_{T_i} + C|\alpha_S| \|\nabla\varphi_i\|_{T_i}.$$

Since

$$H_i^2 |f_i| \|\nabla\varphi_i\|_{T_i} = \left(\int_{T_i} |\nabla\varphi_i|^2 f_i^2 H_i^4 \right)^{\frac{1}{2}} \leq C \left(\int_{T_i} H_i^2 f_i^2 \right)^{\frac{1}{2}},$$

the desired bound (4.4) follows at once. This completes the proof. \square

Now we can state and prove a global lower bound for the error decrease.

COROLLARY 4.3. *Let \mathcal{T}_H and \mathcal{T}_h be triangulations of Ω satisfying (3.1). Then we have the following global lower bound for the error reduction*

$$\|u_h - u_H\|_{\Omega}^2 \geq \frac{\theta^2}{2C_4 C_1} \|u - u_H\|_{\Omega}^2 - \frac{C_5}{C_4} \text{osc}(f, \mathcal{T}_H)^2.$$

Proof. By Lemma 4.2 and step 1 of Marking Strategy E we have

$$\begin{aligned} \theta^2 \eta_H^2 &\leq \sum_{S \in \mathcal{S}_H} \eta_S^2 \leq C_4 \sum_{S \in \mathcal{S}_H} \|u_h - u_H\|_{\Omega_S}^2 + C_5 \sum_{S \in \mathcal{S}_H} \|H(f - f_H)\|_{\Omega_S}^2 \\ &\leq 2C_4 \|u_h - u_H\|_{\Omega}^2 + 2C_5 \|H(f - f_H)\|_{\Omega}^2. \end{aligned}$$

Hence,

$$\|u_h - u_H\|_{\Omega}^2 \geq \frac{\theta^2}{2C_4} \eta_H^2 - \frac{C_5}{C_4} \|H(f - f_H)\|_{\Omega}^2,$$

and the assertion follows from (1.3) and Lemma 2.1. \square

Lemmas 4.1, 4.2, and Corollary 4.3 have provided us with the necessary tools to prove Theorem 3.1.

Proof of Theorem 3.1. In view of Lemma 4.1 and Corollary 4.3, we have

$$\begin{aligned} \|u - u_h\|_{\Omega}^2 &= \|u - u_H\|_{\Omega}^2 - \|u_H - u_h\|_{\Omega}^2 \\ &\leq \|u - u_H\|_{\Omega}^2 \left(1 - \frac{\theta^2}{2C_4 C_1} \right) + \frac{C_5}{C_4} \text{osc}(f, \mathcal{T}_H)^2. \end{aligned}$$

Assume now that $\|u - u_H\|_{\Omega} > \epsilon$. Since $\text{osc}(f, \mathcal{T}_H) \leq \mu\epsilon$, then

$$\|u - u_h\|_{\Omega}^2 \leq \|u - u_H\|_{\Omega}^2 \left(1 - \frac{\theta^2}{2C_4 C_1} + \frac{C_5}{C_4} \mu^2 \right).$$

Therefore,

$$\|u - u_h\|_{\Omega} \leq \alpha \|u - u_H\|_{\Omega}$$

where $\alpha := \left(1 - \frac{\theta^2}{2C_4 C_1} + \frac{C_5}{C_4} \mu^2 \right)^{1/2} < 1$ provided $\mu > 0$ is sufficiently small. \square

5. Numerical experiments. We start with a brief discussion of crucial implementation issues, and conclude with three relevant experiments which corroborate convergence of Algorithm C without mesh preadaptation, produce quasi-optimal meshes, and show a very competitive performance.

5.1. Implementation of Algorithm C. Convergent Algorithm C is implemented within the finite element toolbox ALBERT [11, 12]. For the implementation of this algorithm, we have to change the standard adaptive solver for elliptic problems of ALBERT slightly. The following modules are added to, or replace modules of, the standard solver. They are all minor modifications.

Interior nodes. During the refinement of a marked element we have to ensure that one node in the interior and nodes in all sides of the element are created. ALBERT uses recursive bisectioning refinement: the newest-vertex refinement in two dimensions [10] and the algorithm of Kossaczky [9] in three dimensions. This leads to a sequence of *nested* grids, which is crucial in obtaining the error orthogonality of Lemma 4.1.

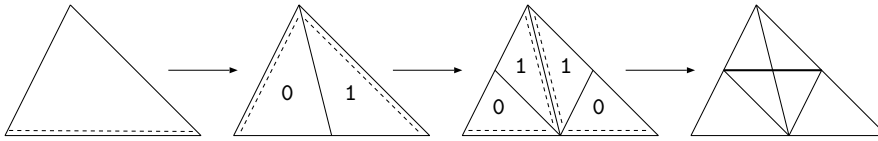


FIG. 5.1. Refinement of triangles in two dimensions by newest-vertex bisection. Dashed lines indicate the refinement edges.

Creating interior nodes is rather easy in two dimensions. First, elements are marked for two bisections and then refined. This already produces a node at the midpoint of each edge. Second, the two grandchildren with index 1 are bisected once more. The whole refinement process is shown in Figure 5.1. The first refinement step may, as usual, involve surrounding elements which are not marked. This is an inevitable effect in order to preserve mesh conformity. The second refinement step is *local* in that it involves only the two grandchildren with index 1 and does not spread outside them.

In three dimensions it is impossible to perform the second step by dealing only with children of the original tetrahedron. The first step consists of three bisections. In order to obtain the interior nodes, the second step consists of marking some subtetrahedra for two or three additional bisections. This has the spreading effect of creating additional nodes in the edges of the original tetrahedron. For the implementation, we do not split the refinement into two steps, but rather mark a tetrahedron for six bisections which are performed in one step. This creates an interior node in the tetrahedron and interior nodes in all the element faces. Example 5.4 demonstrates experimentally that the additional nodes are not too many and the resulting meshes are still quasi-optimal.

Side-based error estimator In view of (2.6), we mark sides for refinement. Usually, error indicators are stored elementwise and marking is also done elementwise. These modules are now changed in such a way that the jump residual $\|H_S^{1/2} J_S\|_S$ across a side S and the element residual $\|H f\|_{\Omega_S}$ of the two adjacent simplices are stored at the side S itself. The marking function thus uses side error indicators η_S and marks both adjacent elements for refinement.

According to Marking Strategy E, we collect sides in $\hat{\mathcal{S}}_H$ with biggest side error indicators η_S until

$$\left(\sum_{S \in \hat{\mathcal{S}}_H} \eta_S^2 \right)^{1/2} \geq \theta \eta_H.$$

In order to avoid a complicated sorting algorithm for the ordering of the error indicators, we adapt the algorithm proposed in [4].

ALGORITHM 5.1 (Marking algorithm). Let $0 < \theta, \nu < 1$ be given parameters, where $\theta \approx 0.5$ and $\nu \approx 0.1$:

```

 $\eta_{\max} := \max(\eta_S, S \in \mathcal{S}_H)$ 
sum := 0
 $\gamma := 1$ 
while sum <  $\theta^2 \eta_H^2$  do
   $\gamma := \gamma - \nu$ 
  for all  $S$  in  $\mathcal{S}_H$  do
    if  $S$  is not marked
      if  $\eta_S > \gamma \eta_{\max}$ 
        mark both adjacent simplices for refinement
        sum := sum +  $\eta_S^2$ 
      end if
    end if
  end for
end while

```

An alternative to the side-based marking uses element-stored indicators as follows: an element is marked together with all its neighbors. This leads to a slightly larger number of marked elements but may again be viewed as a looking ahead strategy. An advantage is that only the marking strategy has to be modified.

Data oscillation. The last module we supply is a function which marks elements due to data oscillation, i.e., an implementation of Marking Strategy D. For each simplex T , we compute the mean value f_T of f on T and store the value $\|H(f - f_T)\|_T$. Given $\hat{\theta}$ and $\hat{\mathcal{T}}_H$, the set of marked elements by Algorithm 5.1, we enlarge $\hat{\mathcal{T}}_H$ in such a way that

$$\text{osc}(f, \hat{\mathcal{T}}_H) \geq \hat{\theta} \text{osc}(f, \mathcal{T}_H)$$

holds. If this inequality is satisfied by $\hat{\mathcal{T}}_H$, we are done. Otherwise, we use a slight modification of Algorithm 5.1 to mark additional elements. This is now done elementwise using the oscillation $\|H(f - f_T)\|_T$ of f as an indicator.

Quadrature. Computations involving integrals of (nonconstant) f and the exact solution u , such as the right-hand side of the linear system, data oscillation terms and errors, use a quadrature rule of order 7. Exact integration was used for the construction of stiffness matrices and right-hand sides for constant f .

5.2. Example: Crack problem. We consider the domain $\Omega = \{|x| + |y| < 1\} \setminus \{0 \leq x \leq 1, y = 0\}$ with a crack and the exact solution u in polar coordinates

$$u(r, \theta) = r^{\frac{1}{2}} \sin \frac{\theta}{2} - \frac{1}{4} r^2.$$

We solve (1.2) with $A = I$ and $f = 1$, and a nonvanishing Dirichlet boundary condition on $\partial\Omega$. We scale the estimator η_H with the factor 0.25.

We compare the guaranteed error reduction strategy (GERS) of Dörfler [4] with our convergent strategy (CONV). Using GERS, all marked triangles are only bisected twice; the interior node is not created. Since $f \neq 0$ GERS requires an initial mesh refinement to satisfy the mesh fineness condition; since $f \equiv 1$ this initial mesh refinement is a global refinement. Strategy CONV does not need these preadaptation steps; CONV thus starts from a very coarse mesh.

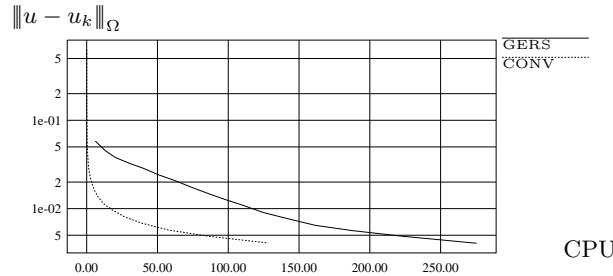


FIG. 5.2. Comparison of CPU time for GERS and CONV.

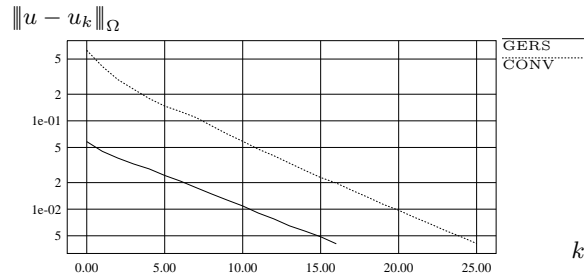


FIG. 5.3. Comparison of reduction rate α^k for GERS, CONV.

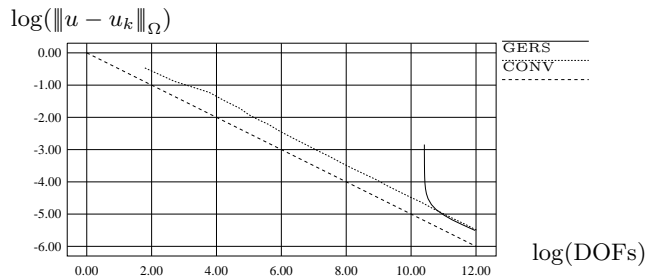


FIG. 5.4. Quasioptimality of GERS and CONV. The optimal decay is indicated by the dashed line with slope $-1/2$.

Figure 5.2 displays a superior performance of CONV in terms of computing time (CPU) due to the coarser initial grid for CONV. From Figure 5.3 we realize that the reduction rate α^k as a function of the iteration number k is comparable for GERS and CONV, the latter being above because CONV starts from a coarser mesh and thus requires more iterations for the same accuracy. Combining both figures we learn that CONV needs more adaptive iterations to reduce the error below the tolerance 0.05 than GERS but only half the CPU time.

Figure 5.4 is quite revealing. It shows the asymptotic relation $\|u - u_k\|_{\Omega} = C \text{DOFs}(k)^{-1/2}$ typical of quasi-optimal meshes in two dimensions and thus of quasi-

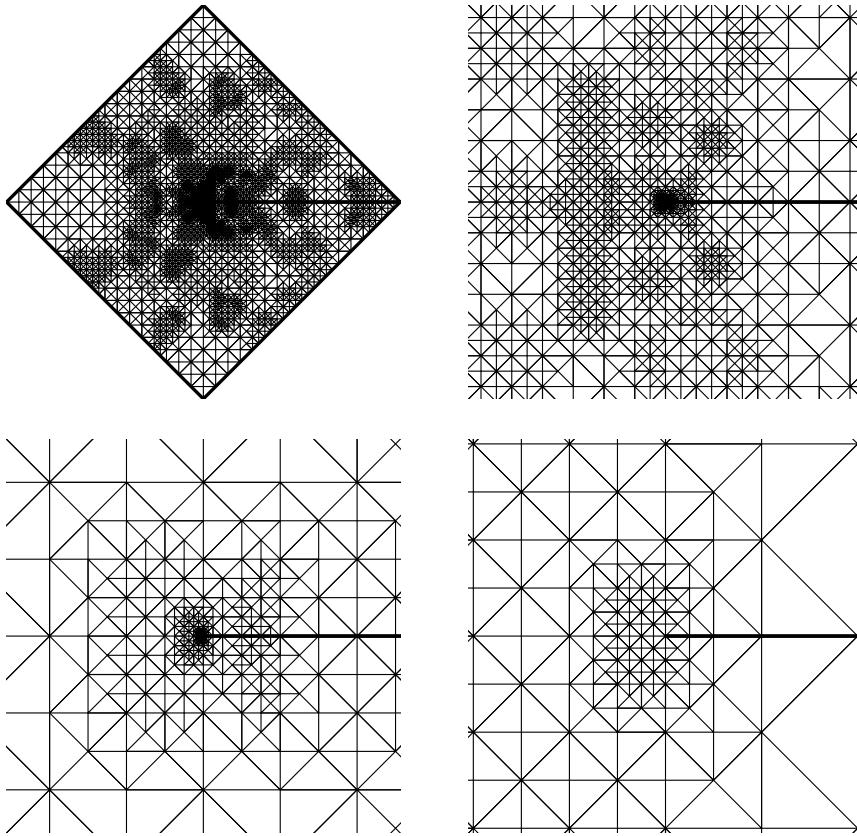


FIG. 5.5. Adaptive grids for iteration 8 of the CONV strategy: full grid (top left), zooms to $(-0.1, 0.1)^2$ (top right), $(-0.01, 0.01)^2$ (bottom left), and $(-0.001, 0.001)^2$ (bottom right).

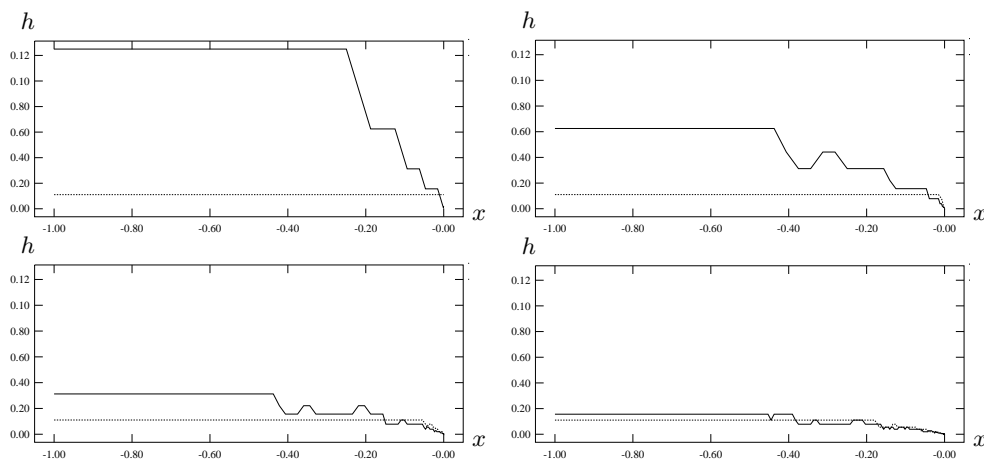


FIG. 5.6. Comparison of local meshsizes h on the line $y = 0$ for GERS (dotted line) and CONV (solid line) on meshes with approximately same errors $\|u - u_k\|_{\Omega}$.

optimal numerical complexity. In the log-log plot the optimal decay of $\|u - u_k\|_\Omega$ is a straight line with slope $-1/2$. This line is also plotted in Figure 5.4.

Figure 5.5 displays the grid of CONV for iteration 8, and three zooms at the origin. The rather strong grading of the quasi-optimal partition is quite apparent.

In order to compare the different local meshsizes for GERS and CONV due to the preadaptation of GERS, we plot the meshsizes along the segment $\{-1 < x < 0, y = 0\}$ in Figure 5.6. We choose the meshes in such a way that the error on the respective meshes is approximately the same for GERS and CONV. The pictures correspond to the meshes in iteration 0 (top left), 4 (top right), 8 (bottom left), and 12 (bottom right) of GERS with errors $\|u - u_k\|_\Omega \approx 5.8\text{e-}02, 2.8\text{e-}02, 1.4\text{e-}02,$ and $7.7\text{e-}03$ and iterations 10, 14, 18, and 22 of CONV with errors $5.8\text{e-}02, 2.7\text{e-}02, 1.3\text{e-}02,$ and $6.8\text{e-}03$. We realize the strong effect of mesh preadaptation needed by GERS: in contrast to CONV, GERS has to reduce the meshsize solely near the origin. This corroborates our claim that mesh preadaptation is unnecessary for constant right-hand sides f .

Finally, we compare CONV with the maximum strategy (MS), which is not known to converge but is the strategy of choice among practitioners. Figure 5.7 depicts a similar performance of both CONV and MS in terms of DOFs.

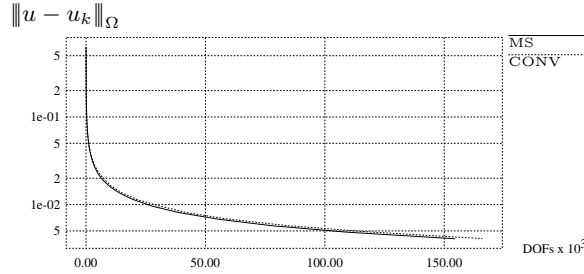


FIG. 5.7. Comparison of CONV and MS.

5.3. Example: Discontinuous coefficients. We invoke the formulas derived by Kellogg [8] to construct an exact solution of an elliptic problem with piecewise constant coefficients and vanishing right-hand side f ; data oscillation is thus immaterial. We now write these formulas in the particular case $\Omega = (-1, 1)^2$, $A = a_1 I$ in the first and third quadrants, and $A = a_2 I$ in the second and fourth quadrants. An exact weak solution u of (1.2) for $f \equiv 0$ is given in polar coordinates by $u(r, \theta) = r^\gamma \mu(\theta)$, where

$$\mu(\theta) = \begin{cases} \cos((\pi/2 - \sigma)\gamma) \cdot \cos((\theta - \pi/2 + \rho)\gamma) & \text{if } 0 \leq \theta \leq \pi/2, \\ \cos(\rho\gamma) \cdot \cos((\theta - \pi + \sigma)\gamma) & \text{if } \pi/2 \leq \theta \leq \pi, \\ \cos(\sigma\gamma) \cdot \cos((\theta - \pi - \rho)\gamma) & \text{if } \pi \leq \theta < 3\pi/2, \\ \cos((\pi/2 - \rho)\gamma) \cdot \cos((\theta - 3\pi/2 - \sigma)\gamma) & \text{if } 3\pi/2 \leq \theta \leq 2\pi, \end{cases}$$

and the numbers γ, ρ, σ satisfy the nonlinear relations

$$(5.1) \quad \begin{cases} R := a_1/a_2 = -\tan((\pi/2 - \sigma)\gamma) \cdot \cot(\rho\gamma), \\ 1/R = -\tan(\rho\gamma) \cdot \cot(\sigma\gamma), \\ R = -\tan(\sigma\gamma) \cdot \cot((\pi/2 - \rho)\gamma), \\ 0 < \gamma < 2, \\ \max\{0, \pi\gamma - \pi\} < 2\gamma\rho < \min\{\pi\gamma, \pi\}, \\ \max\{0, \pi - \pi\gamma\} < -2\gamma\sigma < \min\{\pi, 2\pi - \pi\gamma\}. \end{cases}$$

Since we want to test the algorithm CONV in some worst case scenario, we choose $\gamma = 0.1$, which produces a very singular solution u that is barely in H^1 . We then solve (5.1) for R , ρ , and σ using Newton’s method to obtain

$$R = a_1/a_2 \cong 161.4476387975881, \quad \rho = \pi/4, \quad \sigma \cong -14.92256510455152,$$

and finally choose $a_1 = R$ and $a_2 = 1$. A smaller γ would lead to a larger ratio R , but in principle γ may be as close to 0 as desired.

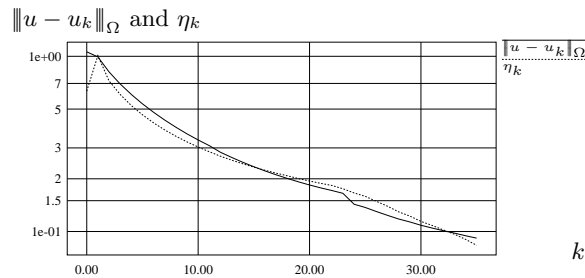


FIG. 5.8. Error reduction: estimate and true error.

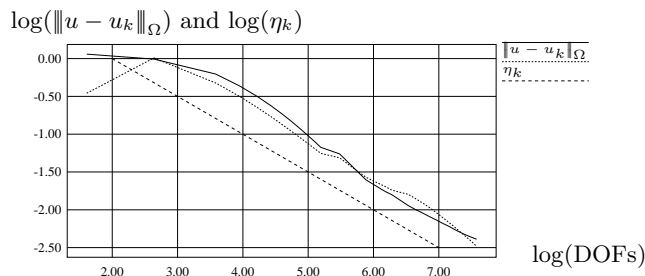


FIG. 5.9. Quasioptimality of CONV: estimate and true error. The optimal decay is indicated by the dashed line with slope $-1/2$.

In Figures 5.8-5.9 we see the same behavior of the true error $\|u - u_k\|_\Omega$ and the estimator η_k scaled by the factor 0.05. Figure 5.9 demonstrates that the grids and associated numerical complexity are quasi-optimal: $\|u - u_k\|_\Omega = C \text{DOFs}(k)^{-1/2}$ is valid asymptotically (the performance of an optimal method is again indicated by the additional straight line).

For this problem the grid is highly graded at the origin. It is worth realizing the strength of the singularity at hand in Figure 5.10. We see a mesh with less than 2000 nodes and three zooms at the origin, each obtained with a magnifying factor 10^3 , and yet exhibiting a rather strong grading. This is also reflected in Figure 5.11, which depicts the graph of the discrete solution over the underlying mesh: the solution is flatter in the quadrants with $a \approx 161$ although the grid is finer, which accounts for the presence of a in the energy norm. This picture was created using the graphics package GRAPE [7]. This example is much more singular than Example 5.2.

5.4. Example: Variable source. In Examples 5.2 and 5.3 the source term is constant. It is our purpose now to examine the effect of data oscillation (1.3). To this end, we consider the domain $\Omega = (-1, 1)^d$ with $d = 2, 3$, and the exact solution

$$u(x) = e^{-10|x|^2}$$

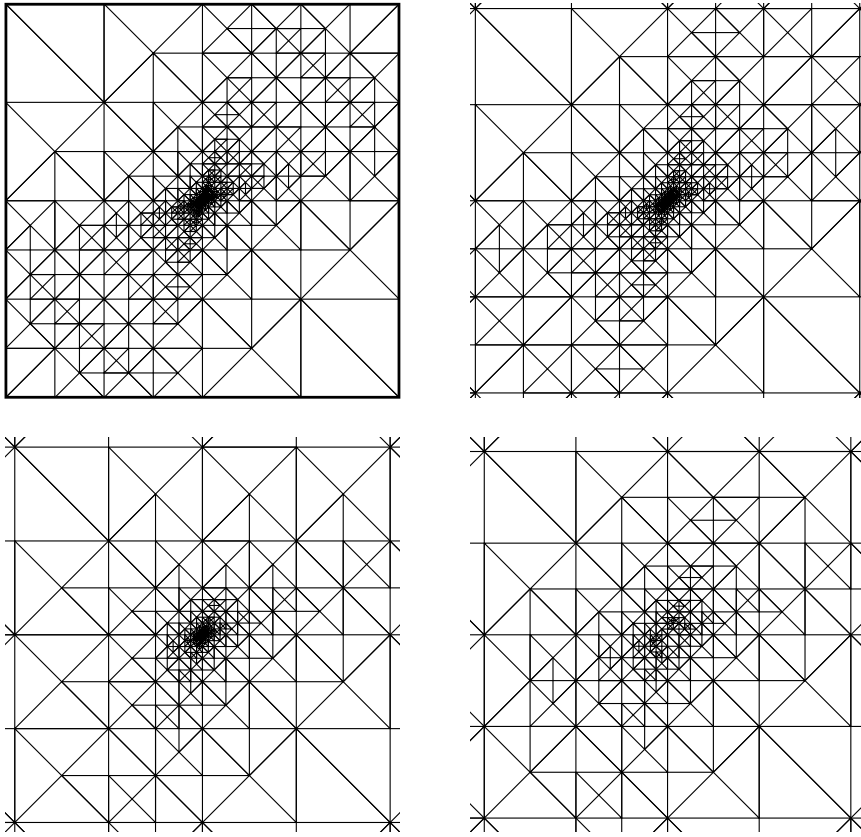


FIG. 5.10. Final grid: full grid with < 2000 nodes (top left), zooms to $(-10^{-3}, 10^{-3})^2$ (top right), $(-10^{-6}, 10^{-6})^2$ (bottom left), and $(-10^{-9}, 10^{-9})^2$ (bottom right).

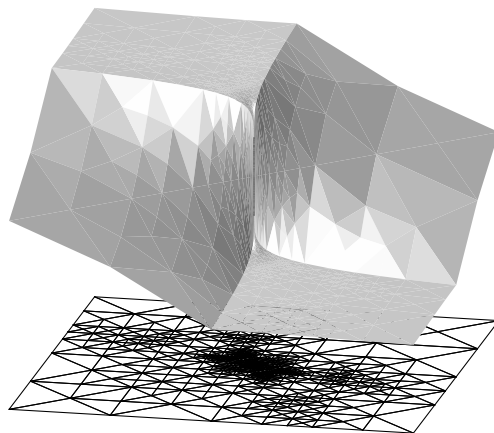


FIG. 5.11. Graph of the discrete solution and underlying grid.

of (1.2) with $A = I$ and nonconstant $f = -\Delta u$. Such an f exhibits a relatively large variation in Ω , and within elements, which forces Algorithm C to refine additional elements due to data oscillation (step 6 of Algorithm C), not yet marked for refinement

TABLE 5.1

Total number and number of marked elements per iteration in two dimensions (left) and three dimensions (right): *est.*: marked elements due to error estimator, *osc.*: additionally marked elements to data oscillation.

iter.	elements	est.	osc.
0	4	8	0
1	64	16	16
2	704	56	8
3	2256	80	0
4	4208	96	8
5	6624	112	24
6	8752	344	0
7	17512	432	0
8	28368	608	0
9	42896	768	16
10	60216	2192	0
11	113040	2296	24
12	160592	3816	24

iter.	elements	est.	osc.
0	6	6	0
1	384	48	0
2	7776	48	48
3	15936	576	0
4	112320	5040	0
5	860592	5136	720
6	1693536	30144	0

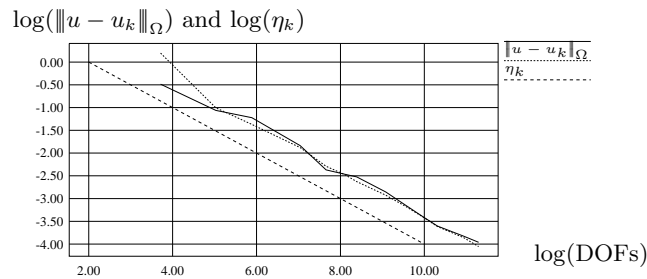


FIG. 5.12. Quasioptimality of CONV: estimate and true error in two dimensions. The optimal decay is indicated by the line with slope $-1/2$.

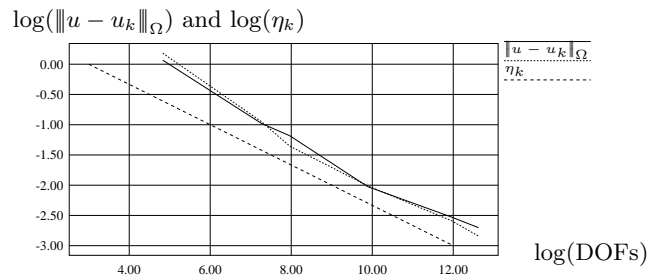


FIG. 5.13. Quasioptimality of CONV: estimate and true error in three dimensions. The optimal decay is indicated by the line with slope $-1/3$.

by Marking Strategy E. This is reported in Table 5.1 for two dimensions (left) and three dimensions (right). We see that the number of additional elements due to large data oscillation is rather small relative to those due to large error indicators, but it is *not* zero. On the one hand, this confirms that control of data oscillation cannot be omitted in a convergent algorithm. On the other hand, this explains why data oscillation seems to play a minor role for (piecewise) smooth data f , and hints at the underlying reasons why most adaptive strategies, although neglecting data oscillation, converge in practice.

As mentioned in section 5.1, we produce in three dimensions the interior node by bisecting a marked tetrahedron six times. This corresponds in two dimensions to

four bisections of a marked triangle, which is used here instead of the procedure of Figure 5.1. Although this produces more DOFs than needed, Figures 5.12 and 5.13 demonstrate that the resulting meshes are still quasi-optimal for both two dimensions and three dimensions. Here, the estimators η_k were scaled by the factor 0.25. For comparison with an optimal mesh, dashed lines with slope $-1/d$ are plotted in Figure 5.12 ($d = 2$) and Figure 5.13 ($d = 3$); note that these lines have the same slope due to different scaling of the y axis.

Finally, in Figure 5.14 we cut $(0,1)^3$ out of the domain $(-1,1)^3$ and show the adaptive grid of the three-dimensional simulation on the boundary of the resulting domain. In the left picture we show the full grid of the 2nd iteration and in the right one a zoom into the grid of the 4th iteration. For this picture we also used the graphics package GRAPE.

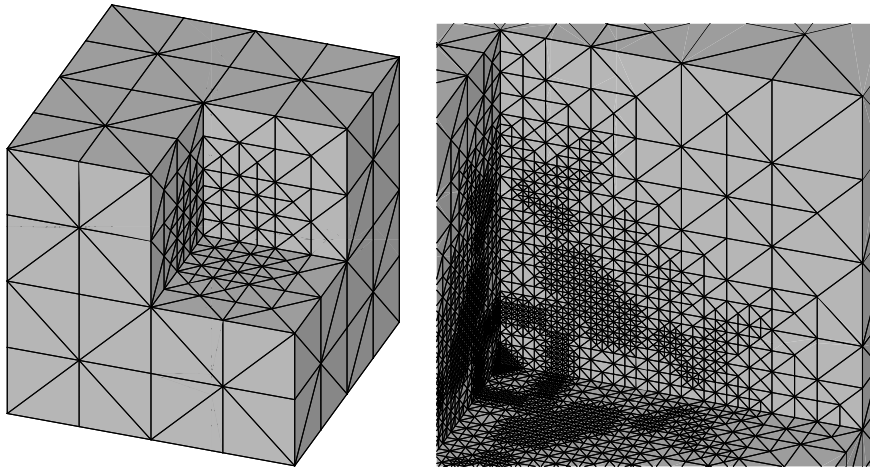


FIG. 5.14. Adaptive grids of the three-dimensional simulation on $\partial((-1,1)^3 \setminus (0,1)^3)$: full grid of the 2nd iteration (left), zoom into the grid of the 4th iteration (right).

REFERENCES

- [1] I. BABUŠKA AND A. MILLER, *A feedback finite element method with a posteriori error estimations: Part I. The finite element method and some basic properties of the a posteriori error estimator*, *Comput. Methods Appl. Mech. Engrg.*, 61 (1987), pp. 1–40.
- [2] I. BABUŠKA AND M. VOGELIUS, *Feedback and adaptive finite element solution of one-dimensional boundary value problems*, *Numer. Math.*, 44 (1984), pp. 75–102.
- [3] A. COHEN, W. DAHMEN, AND R. DEVORE, *Adaptive wavelet methods for elliptic operator equations—Convergence rates*, *Math. Comp.*, to appear.
- [4] W. DÖRFLER, *A convergent adaptive algorithm for Poisson's equation*, *SIAM J. Numer. Anal.*, 33 (1996), pp. 1106–1124.
- [5] W. DÖRFLER, *A robust adaptive strategy for the nonlinear Poisson equation*, *Computing*, 55 (1995), pp. 289–304.
- [6] W. DÖRFLER AND O. WILDEROTTER, *An adaptive finite element method for a linear elliptic equation with variable coefficients*, *ZAMM Z. Angew. Math. Mech.*, 80 (2000), pp. 481–491.
- [7] *GRAPE—GRAphics Programming Environment Manual, Version 5*, SFB 256, University of Bonn, 1995.
- [8] R. B. KELLOGG, *On the Poisson equation with intersecting interfaces*, *Appl. Anal.*, 4 (1975), pp. 101–129.
- [9] I. KOSSACZKÝ, *A recursive approach to local mesh refinement in two and three dimensions*, *J. Comput. Appl. Math.*, 55 (1994), pp. 275–288.

- [10] W. MITCHELL, *A comparison of adaptive refinement techniques for elliptic problems*, ACM Trans. Math. Software, 15 (1989), pp. 210–227.
- [11] A. SCHMIDT AND K. G. SIEBERT, *ALBERT: An Adaptive Hierarchical Finite Element Toolbox*, Documentation, Preprint 06/2000, Universität Freiburg.
- [12] A. SCHMIDT AND K. G. SIEBERT, *Concepts of the Finite Element Toolbox ALBERT*, Preprint 17/1998, Universität Freiburg, Notes Numer. Fluid Mech., to appear.
- [13] R. VERFÜRTH, *A Review of A Posteriori Error Estimation and Adaptive Mesh-Refinement Techniques*, Wiley-Teubner, Chichester, 1996.